Test of predicted gamma stability at spins above $8\hbar$ in ^{64}Zn

B. Crowell,* P. J. Ennis,† C. J. Lister,* and W. R. Schief, Jr.‡
A.W. Wright Nuclear Structure Laboratory, Yale University, New Haven, Connecticut 06511
(Received 25 April 1994)

The nucleus ^{64}Zn is predicted to be γ unstable at low spin, but γ stable at spins of $8\hbar$ and above. In order to see if this structural change is manifested in the decay scheme, this nucleus has been studied via $\gamma\gamma$, recoil-γ, and recoil-$\gamma\gamma$ coincidence techniques using the reaction ^{12}C(^{54}Fe,2p) at 155 MeV. Twenty new levels have been observed with spins of up to $12\hbar$, but no evidence is observed for the predicted onset of gamma stability.

PACS number(s): 23.20.−g, 21.10.Re, 21.60.Ev, 27.50.+e

I. INTRODUCTION

In the past decade, considerable progress has been achieved in predicting the shapes of nuclei using cranked shell-model techniques with Strutinsky renormalization. Although the calculations are less accurate for nuclei whose shapes are soft than for those with stiff minima in the potential energy surface, when the models predict a stiff and well-deformed shape they have seldom been contradicted by experiment. Because of this, the structure of many transitional nuclei, i.e., those between the closed-shell and midshell regions, is far better understood at high spin than in the ground state. The shapes of these nuclei are poorly defined at low spins, and their wave functions are superpositions of rotational, vibrational, and single-particle contributions. They may become much stiffer with the input of large angular momenta, and the wave functions may come to be dominated by rotational components. Examples include superdeformed nuclei in the $A \sim 150$ and $A \sim 190$ regions [1,2] and many nuclei bordering on the $Z = 50$ shell closure [3,4].

The nucleus ^{64}Zn, which has two valence protons and six valence neutrons outside the doubly magic ^{56}Ni core, lies in such a transitional region. At low spins, previous experimental data show that a wide variety of collective degrees of freedom are active. The $0^+, \ldots, 6^+$ sequence of yrast states is linked by highly collective $E2$ transitions, with strengths of 20–30 Weisskopf units (W.u.). This would ordinarily be considered indicative of collective rotation of an ellipsoidally deformed shape, and the measured quadrupole moment [5] of $-0.13(1)$ e b for the yrast 2^+ state is consistent with a prolate deformation of $\beta_2 \approx 0.15$.

This apparent simplicity is misleading. Nuclei in this region are predicted to be quite soft with respect to triaxial and octupole deformations [6], and a more detailed examination of the data reveals that a larger variety of rotational and vibrational degrees of freedom are available in this nucleus at low spins. A brief list of some of the most significant electromagnetic data concerning the low-spin states [5,7–10] is given in Table I. Even this short list of data is sufficient to rule out most simple models. Collective rotation of an axially symmetric shape is inconsistent with the large ratio of $B(E2, 2_2^+ \rightarrow 2_1^+)/B(E2, 2_2^+ \rightarrow 0^+)$, complete gamma instability is ruled out by the large value of Q_2^+, and a well-defined triaxial shape would require an unrealistically large value of β_2 to reproduce Q_2^+. The various collective motions appear to be coupled with each other, and possibly with single-particle excitations, in a complex manner.

The existence of octupole collectivity in this nucleus is demonstrated by the large $B(E3, 3^- \rightarrow 0_1^+)$ value of 23 ± 4 W.u. [7]. Perhaps the only valid simplifying assumption is that the octupole degrees of freedom are irrelevant for understanding the positive-parity states; in a naive picture of harmonic octupole phonon excitations, the two-octupole-phonon multiplet would lie at about 6 MeV, so that all its members would be separated from the yrast line by at least 2 MeV.

Prior to the present experiment, excited states in ^{64}Zn had been observed only at spins of $7\hbar$ and below. In this paper we present experimental data and cranked Nilsson-Strutinsky calculations on the structure of this nucleus at spins of $8\hbar$ and above, and make a detailed comparison of theory and experiment. The calculations predict a marked simplification of the structure of the yrast states.

TABLE I. Previous electromagnetic data on low-spin states in ^{64}Zn.

Q_2^+	=	−0.13	±	0.01	b
$B(E2, 2_1^+ \rightarrow 0_1^+)$	=	23	±	1	W.u.
$B(E2, 2_2^+ \rightarrow 2_1^+)$	=	40	±	4	W.u.
$B(E2, 2_2^+ \rightarrow 0_1^+)$	=	0.25	±	0.02	W.u.
$B(E3, 3^- \rightarrow 0_1^+)$	=	23	±	4	W.u.

*Present address: Argonne National Laboratory, Argonne, IL 60439.
†Present address: AT&T Bell Laboratories, Whippany, NJ 07981-0903.
‡Present address: Dept. of Physics, FM-15, University of Washington, Seattle, WA 98195.

This occurs becuase the rotational alignment of two $g_{9/2}$ neutrons stiffens the core and stabilizes a well-deformed shape with $\gamma \approx 30°$. The calculations also predict that at similar spins, centrifugal effects should stabilize the deformation of the nonaligned states, leading to a well-defined deformed minimum in the potential energy surface with $\gamma \approx 0$. The calculations will be discussed in detail below. Experimental evidence has been presented for similar effects, involving both neutron and proton $(g_{9/2})^2$ configurations, in some neighboring nuclei [11], but the situation in ^{64}Zn should be simpler, since the proton $g_{9/2}$ shell is too far from the Fermi surface to be energetically available. The purpose of this paper is to present the new data on states above $8\hbar$, and to compare them with the calculations to determine whether well-defined rotational bands exist as predicted by the calculations. The low-spin structure will also be discussed in light of the new calculations.

II. EXPERIMENT

A. Experimental techniques

Excited states of ^{64}Zn were formed in the reaction ^{12}C(^{54}Fe,2p) at 155 MeV, using beams provided by the NSF tandem accelerator at Daresbury. The target was a 450 μg/cm^2 natural carbon foil. Gamma rays were detected by the POLYTESSA spectrometer, consisting of 19 Compton-suppressed Ge detectors, 15 of them in rings of five each at 40, 117, and 143 degrees with respect to the beam, and four at 101 degrees. The Ge detectors were gain-matched in hardware for Doppler-shifted peaks ($v/c = 0.063$). The broadening of the peaks in the gamma-ray spectra (Figs. 1 and 2) is due to the width of the velocity distribution of the recoiling nuclei. The nuclei produced in reactions recoiled into the Daresbury recoil separator, which dispersed them according to A/Q, and they were then detected in the three anodes of the ionization chamber at the focal plane, whose E, ΔE_1, and ΔE_2 parameters allowed separation according to Z.

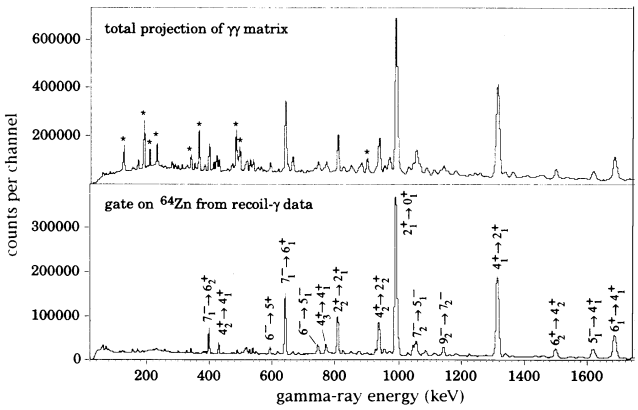

FIG. 1. Total projection of $\gamma\gamma$ data and gate on ^{64}Zn from recoil-γ data. The transitions labeled with asterisks are contaminants from ^{64}Ga, which are all eliminated through the gate on ^{64}Zn recoils.

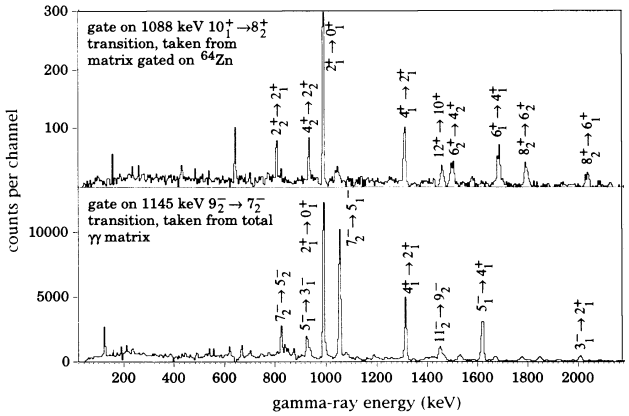

FIG. 2. Gates on high-spin transitions in ^{64}Zn.

The trigger for recording an event was a coincidence between two Ge detectors ($\gamma\gamma$ events) or between at least one Ge detector and the ionization chamber (recoil-γ events). Detailed information on the experimental techniques have been presented in Ref. [6], which describes the level structure of the $N = Z$ nucleus ^{64}Ge, produced with a partial cross section of 0.6 mb in the same experiment. The nucleus ^{64}Zn was the most prolifically produced product of the reaction, with a partial cross section which was larger by a factor of 250 than that for ^{64}Ge. A total of 60 million $\gamma\gamma$ events was acquired, of which 1.3 million were recoil-$\gamma\gamma$ events tagged with a ^{64}Zn recoil. A total of 39 million recoil-γ coincidences was recorded involving ^{64}Zn.

Two-dimensional histograms of E_γ versus E_γ were used to construct the level scheme. One such histogram was created with a gate on ^{64}Zn recoils, and another without any gate on the recoil data. Figures 1 and 2 show examples of some gamma-ray spectra observed in this experiment. Comparison of the total projection of the γ-γ coincidence data with the total spectrum gated on ^{64}Zn recoils demonstrates the great usefulness of the recoil-γ data for obtaining clean spectra. The statistics in the recoil-γ-γ data-set were sufficient to allow the study of transitions, such as the 1088 keV transition shown in Fig. 2, with intensities of as little as 3% of that of the $2^+ \rightarrow 0^+$ transition in ^{64}Zn. In some cases, extremely weak transitions, such as the 1454 keV $11^- \rightarrow 9^-$ transition seen in Fig. 2(b), which has an intensity of only 0.6% of that of the $2^+ \rightarrow 0^+$ transition, were more easily studied in the γ-γ data without any gate on recoils. The two data-sets were highly complementary, and the choice of one or the other depended mainly on whether any significant contamination from other reaction channels was present in a given gate.

For some strong transitions, intensities and angular distributions were extracted from the recoil-γ data, using the total spectrum in each ring of detectors gated on recoils of ^{64}Zn. For transitions that can be resolved in gamma singles, this provides higher statistics and minimizes the bias imposed by the response of the detection system, which would be greater in gamma-gamma coincidence data. The transitions for which this was done are annotated accordingly in Table II. The angular distribu-

TABLE II. Energies and intensities of transitions in ^{64}Zn.

E_γ (keV)	I_γ	Notes	DCO ratio	a_2	Multi-polarity	Initial state	Final state
340.8(4)	0.50(1)	a,c			$M1+E2$	4_3^+	4_2^+
397.8(2)	4.21(1)	a,c	0.64(2)		$E1$	7_1^-	6_2^+
429.4(4)	1.4(1)				$M1+E2$	4_2^+	4_1^+
512.2(2)	4.5(5)	c	0.36(2)		$M1+E2$	6^-	5_2^-
516.8(1)	0.8(1)				$M1+E2$	7_3^-	7_1^-
547.8(1)	0.08(2)					7	7_3^-
592.4(1)	2.47(2)	a,c	0.63(2)		$E1$	6^-	5^+
641.36(4)	18.4(1)	c	0.66(2)	−0.163(5)	$E1$	7_1^-	6_1^+
744.1(1)	4.39(2)	a,c	0.75(3)			6	5_1^-
770.8(1)	4.46(2)	a,c			$M1+E2$	4_3^+	4_1^+
807.67(1)	18.10(3)	a			$M1+E2$	2_2^+	2_1^+
824.7(1)	8.2(8)				$E2$	7_2^-	5_1^-
838.3(3)	0.28(2)	a				8	9^-
927.6(1)	1.98(2)	a,c			$E2$	5_1^-	3^-
937.3(3)	16.9(4)	a,c			$E2$	4_2^+	2_2^+
954.8(1)	2.39(2)	a	0.92(3)		$E2$	8	6
991.8(1)	100	c	0.90(1)	+0.124(2)	$E2$	2_1^+	0_1^+
997.6	0.8(1)	b			$E2$	10_1^+	8_3^+
1000.7(5)	1.60(4)	c			$M1+E2$	5^+	4_3^+
1030.4(1)	1.19(2)	a				7	6
1047.2(5)	4.3(1)	a			$E2$	9^-	7^-
1056.6(7)	8.1(5)	c	0.91(1)		$E2$	7^-	5_1^-
1064.5(5)	1.2(1)		0.9(2)			7	7_1^-
1079.4(6)	0.66(2)	c			$E1$	5^-	4_3^+
1088.4(2)	3.2(1)	a	0.96(7)	+0.45(2)	$E2$	10_1^+	8_2^+
1144.6(1)	4.0(3)		0.91(1)		$E2$	9^-	7_2^-
1183.0(3)	0.93(4)		0.92(6)		$E2$	10_1^+	8_1^+
1189.4(3)	0.09(1)		0.9(1)		$E2$	12_2^+	10_2^+
1210.7(3)	0.35(3)		1.2(2)		$E2$	10^+	8_3^+
1227.3(2)	1.4(2)		0.92(2)		$E2$	7_2^-	5_1^-
1263.4(5)	0.10(2)		0.52(6)			8	7
1315.3(1)	76.7(2)	a,c	0.88(1)	+0.235(3)	$E2$	4_1^+	2_1^+
1341.5(1)	4.89(5)	a,c			$M1+E2$	5^+	4_2^+
1454.3(2)	0.6(1)		0.98(3)		$E2$	11^-	9^-
1463.7(3)	0.57(2)		0.86(6)		$E2$	12_1^+	10_1^+
1500.6(1)	9.95(4)	a,c			$E2$	6_2^+	4_2^+
1581.7(4)	1.45(3)	a					9^-
1619.8(1)	15.25(5)	a,c	0.67(1)		$E1$	5_1^-	4_1^+
1627.2(6)	1.8(1)						7^-
1686.8(1)	34.3(2)	a,c	0.89(1)	+0.250(5)	$E2$	6_1^+	4_1^+
1746.4(5)	0.92(5)				$E2$	4_2^+	2_1^+
1771.5(2)	1.4(2)	c			$M1+E2$	5^+	4_1^+
1796.2(3)	1.2(1)				$E2$	8_2^+	6_2^+
1799.1(1)	5.89(3)	a			$E2$	2_2^+	0_1^+
1851.6(3)	2.0(2)	c			$E1$	5^-	4_1^+
1869.9(7)	0.35(2)		1.0(2)		$E2$	10_2^+	8_1^+
1887.0(4)	0.5(1)		2.1(6)		$E2$	8_2^+	6_1^+
1915(2)	0.09(2)		1.3(3)		$E2$	10_3^+	8_2^+
1943.7(3)	3.7(1)	a		+0.21(2)	$E2$	8_1^+	6_1^+
2007.9(3)	3.50(3)	a,c	0.63(3)	−0.24(2)	$E1$	3^-	2_1^+
2038.9(5)	1.8(1)	a	0.88(6)	+0.30(4)	$E2$	8_2^+	6_1^+
2087.8(7)	3.49(3)	a,c	0.89(3)		$E2$	4_3^+	2_1^+
2130.6(6)	2.6(1)	a	0.91(6)	+0.19(3)	$E2$	8_3^+	6_1^+
2221(2)	0.14(3)		0.8(2)		$(E2)$	(10^+)	8_1^+

[a]Intensity based on recoil-γ data.

[b]Transition is a doublet. Energy inferred from differences of energies of other, interlocking transitions. Intensity determined from coincident intensities of other transitions.

[c]Multipolarity was established by previous work.

tions were fit to the functional form $A_0[1 + a_2P_2(\cos\theta)]$, with the coefficient A_0 measuring the intensity, and a_2 the angular distribution. The statistical error bars for the intensities of many of these transitions were quite small. For example, the 992 keV $2^+ \rightarrow 0^+$ peak contained 3.5 million counts in the total recoil-γ spectrum. The systematic errors of ~10% in the efficiency calibration were therefore dominant in most of these cases. Estimates of these systematic errors were difficult to determine, and therefore have not been included in the table.

Almost all of the new transitions in the level scheme were too weak to allow the direct analysis of angular distributions. The multipolarities of these transitions were instead determined by the use of DCO ratios (directional correlations of oriented nuclei). These were defined in terms of the coincident intensities according to

$$R_{\mathrm{DCO}}(\gamma_1) \equiv \frac{\sum_{\theta_1=40^\circ,143^\circ} I(\gamma_1,\theta_1;\gamma_2,\theta_2)}{\sum_{\theta_1=101^\circ,117^\circ} I(\gamma_1,\theta_1;\gamma_2,\theta_2)} ,$$

where both sums also run over all four values of θ_2. In principle ratios such as these depend on the multipolarities λ_1, λ_2 of the two transitions [12]. The transitions depopulating the newly observed states, however, all have spins large enough that angular correlation effects are small [13], and λ_1 therefore determines their DCO ratios, with little sensitivity to λ_2. Empirically, in the present experiment, transitions previously determined to be quadrupoles had $R_{\mathrm{DCO}} \approx 0.9$, while pure dipoles had $R_{\mathrm{DCO}} \approx 0.6$. Corrections were applied to account for the differing dead-times of the four rings, and the different efficiency curve of the ring at 40°, whose detectors were constructed in a different geometry. DCO ratios are listed in Table II only where they serve to determine the spins of newly observed levels, or in a few cases to allow a comparison with the angular distribution data.

B. Level scheme and spin and parity assignments

The level scheme constructed from the data is shown in Fig. 3. Because of the interlocking pattern of transitions, most of their placements in the level scheme are unambiguously determined, but the orderings of the 1189-1870 and 1582-1047 sequences are based only on their intensities. Although an effort has been made to impose order on the level scheme by arranging the states into vertical sequences resembling rotational bands, this should be taken mainly as a visual aid; it will be seen below that the application of rotational models is not entirely successful in interpreting the structure of ^{64}Zn.

Table II shows the energies, intensities, and angular distributions of the transitions observed. The intensities of most of the gamma-ray transitions were determined from the $\gamma\gamma$ and recoil-$\gamma\gamma$ data. A possible systematic error was involved in extracting gamma-ray intensities from coincidence data when the efficiency calibration has been obtained with radioactive sources using events composed of single gamma rays. The error arises from the intrinsic dependence of the timing resolution of a Ge detector on the gamma-ray energy, especially for low-energy transitions, since one must introduce a gate on a TAC peak. Based on the requirement of conservation of flux in the level scheme of ^{64}Zn, it was determined that the above effect was negligible (compared to the accuracy of the efficiency calibration) even for the lowest transition energies observed in this experiment.

The nuclei recoiling with $v/c = 0.06$ were within the collimation of the Ge detectors for only ~ 1 ns, so transitions depopulating long-lived states were drastically attentuated. Thus, throughout this level scheme, $\lambda = 3$ assignments can be ruled out. $M2$ multipolarities cannot be excluded on the same grounds, except for the lowest-energy transitions, but one would ordinarily expect competing $E1$ transitions to exist, causing the $M2$ transitions to have small branching ratios.

The spins and parities of all the states labeled in Fig. 3 as having positive parity and even spins greater than $6\hbar$ were determined by the measured DCO ratios, which indicate that they are depopulated through stretched quadrupole transitions leading to states with known spins and parities. The spins and parities assigned to the newly observed 7_3^-, 9_1^-, 9_2^-, and 11^- states likewise are de-

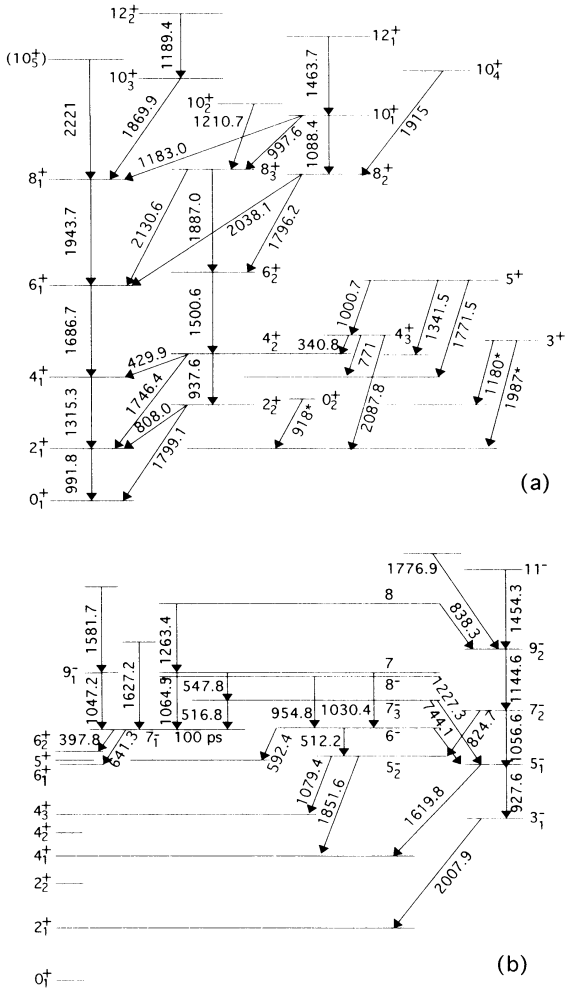

FIG. 3. Level scheme of ^{64}Zn: (a) positive-parity levels; (b) negative-parity levels.

termined by their connections to known states through quadrupole transitions. (As is always the case in angular correlation measurements in reactions induced by heavy ions, nonstretched decay cascades cannot be definitively excluded, but no evidence for such behavior was found.)

The assignment of spin 7 to the state at 5700 keV follows from the fact that it decays to both a 7^- state (through $E_\gamma = 1064$ keV) and a state with spin 6 (via $E_\gamma = 1030$ keV), and the 1064 keV line has a DCO ratio which indicates $\Delta J = 0$ or $\Delta J = \pm 2$. The state at 5700 keV cannot have spin 9, since the 1030 keV transition would then have $\lambda = 3$, and the state would not decay within view of the detectors due to its long lifetime. Spin 5 is also implausible, because the state at 6963 keV, which decays to the 5700 keV state through the 1263 keV dipole transition, would then have to have spin 6, which would make it 3.0 MeV above the yrast line, and therefore unlikely to be populated in heavy-ion reactions with any measurable intensity. The only remaining possibility is that the 5700 keV state has spin 7. The above reasoning also shows that the state at 6963 keV, decaying via the 1263 keV transition, has spin 8.

The spin and parity of the 6^- state at 3899 keV is determined by the fact that it decays to a 5^+ state ($E_\gamma = 592$ keV) and a 5^- state ($E_\gamma = 512$ keV), and the latter transition has a DCO ratio indicative of a mixed $M1/E2$ transition with a large mixing ratio. The state at 4854 keV, which decays to the 6^- state through the 955 keV quadrupole transition, is therefore an 8^- state.

III. CALCULATIONS

A. Strutinsky calculations

Cranked Nilsson-Strutinsky calculations were carried out for ^{64}Zn using the computer code described in Ref. [14]. The calculations employed the standard Nilsson parameters of Ref. [15]. Pairing correlations were incorporated using the BCS theory, with $G_n \times A = 18$ MeV and $G_p \times A = 21$ MeV, and orbitals within 8 MeV of the Fermi level were included in the pairing calculations. Virtual interactions were removed according to the procedure described in Ref. [14], allowing a reliable transformation of the body-fixed quantities E' and ω (total Routhian and rotational frequency) into the corresponding quantities in the laboratory frame, E and $\langle J_x \rangle$. The deformations ε_2, ε_4, and γ were varied self-consistently in order to minimize the total energy at each fixed, integer value of $\langle J_x \rangle$. States of definite particle number were projected out of the BCS wave functions before variation.

The calculated energy levels of the even-spin, positive parity states are compared in Fig. 4 with the observed levels, and with the shell-model calculations of Ref. [16]. The agreement between the Nilsson-Strutinsky calculations and the data is surprisingly good, considering that ^{64}Zn is a transitional nucleus and that the calculations contain no adjustable parameters whatsoever, except for standard parameters which have been determined previously by global fits throughout the periodic table.

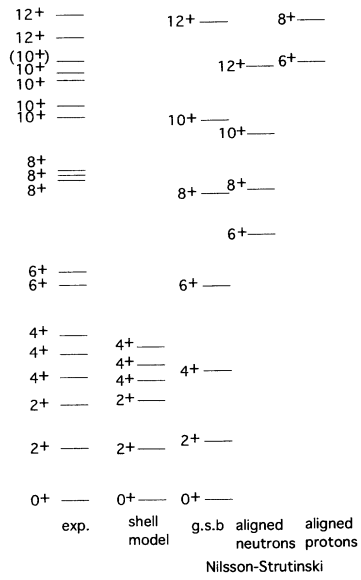

FIG. 4. Comparison of observed and theoretically calculated energy levels for ^{64}Zn.

B. Low-spin positive-parity states

Although cranking wave functions cannot be used directly to compute electromagnetic matrix elements, since they are not states of definite spin, the model can be used to predict quadrupole moments and $E2$ transition rates in the sense that it predicts the shape of the nucleus, which can be related to the electromagnetic quantities through well-known semiclassical formulas. The quadrupole moment of the first excited 2^+ state, with a self-consistently determined prolate deformation of $\epsilon = 0.14$ and $\gamma = 0$, is predicted to be $Q_{\rm intr} = +0.49\ e$ b. This implies a quadrupole moment in the laboratory frame of $Q = -\frac{2}{7}Q_{\rm intr} = -0.14\ e$ b (assuming $K = 0$), in good agreement with the measured value of $-0.13(1)\ e$ b. The magnetic moment of this state, which in cranking calculations for zero-quasiparticle states can be associated with the contribution of the protons to $\langle J_x \rangle$, is calculated to be $+0.96\ \mu_N$ (similar to $2 \times Z/A = 0.94$) reproducing the experimentally observed value [5] of $+0.88(13)$ μ_N to within statistical errors. The agreement with the experimentally determined $B(E2)$ values in the yrast sequence [8–10] is not as good; significantly larger static deformations ($\varepsilon \approx 0.20$–0.25) would be required to reproduce these measurements. Strutinsky calculations with a Woods-Saxon potential [17,18] predict deformations in this range, but it is clear that the value of Q_{2^+} relative to the measurements of $B(E2)$ cannot be exactly reproduced in a rotational model with static deformation.

The potential energy surfaces, are however, extremely soft in ε and γ, and the effects of shape fluctuations on these quantities cannot be ignored. Calculations with a Woods-Saxon potential [18] predict extreme gamma softness as well, with an oblate-prolate energy difference of only ~ 0.1 MeV. For such an extremely gamma-soft nucleus, small quadrupole moments, large $B(E2)$ values, and level spaced according to a $J(J+6)$ pattern are tra-

ditionally expected.

The above arguments can be quantified, following the treatment of Ref. [19]. The collective modes of the nucleus are modeled in a rank-2 tensor describing a quadrupole shape plus three Euler angles describing the orientation of the nucleus. The system is quantized, and a model Hamiltonian, similar to the Bohr Hamiltonian, is constructed from the lowest-order rotationally invariant quantities which can be formed from the quadrupole tensor. The fluctuations in gamma and beta are therefore treated fully, on the same footing as the rotational degrees of freedom. A Hamiltonian, expressed in the principal-axis coordinates, which mimics the calculated potential energy surfaces is

$$H = A\beta^2 + B\beta^4 + \frac{1}{D}[\pi \times \pi]^{(0)} ,$$

where we have assumed a totally gamma-soft potential energy surface, but the tensor π includes all five conjugate momenta, corresponding to beta, gamma, and the three Euler angles. A choice of $A = -267$ MeV and $B = 5930$ MeV produces a potential with its minimum at $\beta = 0.15$, as determined from the cranking calculations, and a beta stiffness similar to that suggested by the calculations. Choosing an inertial parameter $D \approx 40$ MeV gives the best approximation to the apparent moment of inertia for spins between zero and $6\hbar$. This Hamiltonian was diagonalized numerically using the computer code described in Ref. [19]. The results destroy the apparently good agreement obtained between the Strutinsky calculations and the observed characteristics of the low-spin positive-parity states.

A summary of the some of the most physically transparent results is given in Table III. The quantity which most clearly shows the essential problem is the quadrupole moment, which should vanish for a gamma-unstable nucleus in all its excited states, but which is observed in ^{64}Zn to be rather large. The quantity $S(4,3,2)$ is defined as [20]

$$S(4,3,2) \equiv \frac{[E(4_2^+) - E(3^+)] - [E(3^+) - E(2_2^+)]}{E(2_1^+)}$$

and is a measure of the degree of gamma softness, varying from $+1.7$ for a rigid triaxial shape to -2.0 for a gamma-unstable nucleus. The experimental and theoretical values for ^{64}Zn are both indicative of gamma instability. The measured ratio $B(E2, 2_2^+ \rightarrow 2_1^+)/B(E2, 2_2^+ \rightarrow 0_1^+)$, however, is in disagreement with the calculations for a gamma-unstable potential, and would be more typical of a stable triaxial shape with $\gamma \approx 30°$ [21].

The correct incorporation of the fluctuations has not led to an improved reproduction of the data. Even the approximate agreement obtained under the assumption of a rigid shape has now been lost. The most likely reason for these difficulties is that the shape of the potential energy surfaces calculated by the Strutinsky method is incorrect. The possible causes for this will be discussed below, after examining the high-spin states.

C. High-spin positive-parity states

For the low-spin states discussed above, it is perhaps possible to entirely avoid approximate methods such as the cranked Strutinsky approach; as shown in Fig. 4, the shell-model calculations of Ref. [16] give a very good description of the low-spin energy levels. [Qualitative agreement with the observed $B(E2)$ rates was also achieved, although difficulties were encountered in determining an appropriate set of effective charges applicable to all the Zn isotopes.] Unfortunately, for the high-spin states observed in this experiment, a reasonable shell-model treatment would clearly require a much larger model space, including the $g_{9/2}$ neutron shell. As pointed out in Ref. [22], a full shell-model calculation in the traditional sense for open-shell nuclei in this region would require the diagonalization of Hamiltonians with $\sim 10^{12}$ matrix elements, so such an approach is clearly not presently feasible. Modifications of the traditional shell model, such as variational Monte Carlo techniques [22], are promising for dealing with this region, but are still being developed.

It is therefore of some interest that the Strutinsky calculations predict much more gamma-stiff minima for both the rotation-aligned neutron $(g_{9/2})^2$ states and also, due to centrifugal effects, the zero-quasiparticle states. Potential energy surfaces are shown in Fig. 5, derived from the cranked Nilsson-Strutinsky calculations described above. (Calculations with a Woods-Saxon mean field give similar predictions [18].) At spins of $8\hbar$ and above, the rotation-aligned neutron $(g_{9/2})^2$ configuration is predicted to have a gamma-stable shape with $\varepsilon \approx 0.25$–0.30 and $\gamma \approx 25$–$35°$. The stabilization of this shape, with a well-defined minimum in the potential energy surface, is due to the shape-driving effects of the $g_{9/2}$ quasiparticles, which have a particle-like character, and therefore prefer a potential which bulges outward, away from the axis of rotation. The minimum for the high-spin

TABLE III. Comparison of selected experimental and calculated quantities.

	Expt.	Nilsson-Strutinsky	Collective quadrupole Hamiltonian
$E(4_1^+)/E(2_1^+)$	2.32	2.22	2.25
$Q2_1^+(e\ \mathrm{b})$	−0.13(1)	−0.14	−0.01
$B(E2, 2_1^+ \rightarrow 0_1^+)$ (W.u.)	23(1)	9	4
$E(2_2^+)/E(2_1^+)$	1.81		2.25
$B(E2, 2_2^+ \rightarrow 2_1^+)/B(E2, 2_2^+ \rightarrow 0_1^+)$	160(30)		1.62
$S(4,3,2)$	−1.43		−1.44

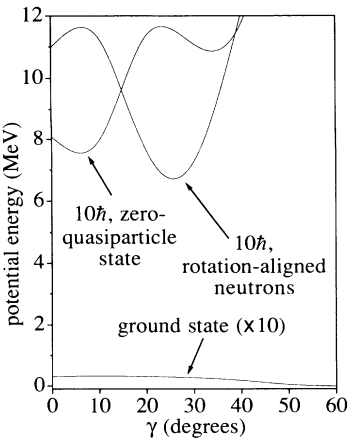

FIG. 5. Potential-energy surfaces calculated as described in the text. Each curve represents the potential energy calculated as a function of the triaxiality parameter γ, for a fixed value of $\langle J_x \rangle$ and a fixed quasiparticle configuration. The curve for the ground state has been stretched vertically by a factor of 10 in order to make visible the very small variations in the potential energy as a function of γ. The parameter γ is defined according to the Lund convention, so that $\gamma = 0°$ corresponds to collective rotation of a prolate shape, and $\gamma = 60°$ represents noncollective rotation of an oblate shape.

zero-quasiparticle states is predicted to have $\varepsilon \approx 0.20$–0.25, $\gamma \approx 0$–$5°$, and is far more gamma stiff than at zero spin, due to the effect of the centrifugal force. (The theoretical error bars for β and γ are due to the flatness of the bottom of the potential, and the ambiguity in separating the aligned configuration from the vacuum configuration, since the two interact through pairing). Since the minima for the two configurations have significantly different values of gamma, they should remain relatively decoupled, resulting in rather pure bands.

The ability to ignore $(g_{9/2})^2$ proton excitations in this nucleus should make the picture significantly simpler than that in the other nuclei in the region which have been studied at similar spins [11]. Although the $g_{9/2}$ proton shell is predicted by both Woods-Saxon and Skyrme-Hartree-Fock calculations to be unbound in ^{64}Zn (see below), the Nilsson potential has no continuum states, so that configurations involving proton $g_{9/2}$ excitations exist within the model. The rotation-aligned proton $(g_{9/2})^2$ states have been included in Fig. 4, but nevertheless, it is clear that they are far too high in energy to be relevant.

The data show that the structure of the positive-parity states in ^{64}Zn becomes, if anything, more complex at high spin. A variety of even-spin positive-parity states is observed, which do not form distinct rotational patterns. The yrast 10^+ state, for example, decays to three different 8^+ states through three transitions with similar energies and branching ratios, and therefore similar $B(E2)$ values. Furthermore, a total of five 10^+ states is observed near the yrast line (including the state at 10 102 keV, whose spin and parity assignment is tentative), which exceeds the number of states which can be accounted for in the model, even allowing for the existence of gamma-vibrational bands built on both configurations. One could perhaps interpret the $12^+ \rightarrow 10^+$ sequence passing through the 1189 keV transition as the expected neutron $(g_{9/2})^2$ band. (Taking the core moment of inertia to be $5\hbar^2$/MeV, the implied rotational alignment is about $8\hbar$, which is appropriate for this configuration.)

However, it is clear that separate, well-defined rotational bands have not emerged near the yrast line. This should be taken as evidence that the cranked Strutinsky technique has failed at high spins in ^{64}Zn, just as it has at low spins. It would be desirable to round out these spectroscopic data on energy levels with data on electromagnetic moments and transition rates at high spins, which might provide a more definite indication of the actual shape of the nucleus. It is unfortunate that measurements of lifetimes would probably not be sufficient to distinguish the zero-quasiparticle states from the rotation-aligned neutron states, since the $B(E2)$ rate varies as $\sqrt{B(E2)} \propto \beta(\cos\gamma - 0.577\sin\gamma)$, which would take on similar values for the vacuum states and the rotation-aligned states. Measurements of the magnetic moments of these states would perhaps be a more sensitive method for singling out the neutron $(g_{9/2})^2$ configuration from the zero-quasiparticle states.

D. Negative-parity states

As discussed in the introduction, the negative-parity states in this nucleus should be expected to be even more difficult to interpret than the positive-parity states, due to the availability to octupole-vibrational modes. The $11^- \cdots 3^-$ sequence connected by the 1454–1145–1057–928 keV cascade exhibits many of the characteristics of a rotational band built on a $K = 0$ octupole-vibrational bandhead, including a collective $B(E3, 3^- \rightarrow 0_1^+)$ value (Table I) and a collective $B(E2, 7^- \rightarrow 5^-) = 21(7)$ W.u. [8–10]. As pointed out in Ref. [6], however, this simple interpretation is not necessarily valid. It is also probable that many of the irregularly spaced sequences of negative-parity states observed at spin 7 and above consist of noncollective quasiparticle excitations.

IV. DISCUSSION

The motivation for this study has been the prediction by cranked Strutinsky calculations that the minima in the potential energy surfaces for ^{64}Zn would be far more stable at high spin that at low spin. The data appear to support exactly the opposite trend. The experimental observables at low spin appear consistent with collective rotational structure of a modestly deformed stable shape, and calculations that include the effect of shape fluctuations give results which are qualitatively inconsistent with the data. The excellent agreement between the data and the calculations without shape fluctuations suggests that there is actually a stiff minimum at low spin, and that the very gamma-soft potential energy surface is in fact stiffer. At high spin, the predicted simplification of the spectra with stiffer minima does not appear. The high-spin structure is not divided into clear rotational

sequences, and is more consistent with a very soft minimum. Although the calculations presented here were carried out with the Nilsson mean field, Woods-Saxon calculations give similar results [18]. We now discuss some of the possible reasons for this disagreement between theory and experiment.

The parameters of the Nilsson and Woods-Saxon single-particle potentials have been fit mainly to the properties of nuclei near doubly closed shells along the line of stability. The application of these mean fields to other nuclei therefore requires interpolation to reach midshell nuclei, and extrapolation to deal with nuclei far from stability. Since ^{64}Zn in a stable nucleus, the extrapolation in N/Z is not a difficulty. In heavy nuclei, interpolation with respect to mass number has worked well. It has been suggested that in light nuclei, the parameters of the Nilsson model might behave in a nonlinear way as a function of the filling of major shells [23,24]. This is certainly possible, since the terms in the Nilsson Hamiltonian reflect a more complicated two-body interaction than would be expected from their simple analytic forms [25], but the parameters proposed in Ref. [24] have not proven any more accurate than the standard ones in typical applications [3]. In addition, the good agreement between the potential energy surfaces calculated using the Woods-Saxon and Nilsson potentials suggests that this is not likely to be the problem. (Although it is possible, for open-shell nuclei, to use Strutinsky calculations to compare the predicted quasiparticle energies in nuclei directly with the exerimentally observed energy levels of odd nuclei [3], the accuracy of the comparison is limited by the accuracy with which the shape can be predicted.) The potential energy surfaces are likely to be most sensitive to the location of the shape-driving neutron $g_{9/2}$ shell relative to the Fermi level. Table IV shows this quantity, and the corresponding quasiparticle energy, for the spherical Nilsson and Woods-Saxon potentials, as well as for the spherical Hartree-Fock potential based on the Skyrme 3 interaction, calculated using the computer code of Ref. [26]. The Woods-Saxon calculations were carried out using the "universal" parameters described in Ref. [17]. The quasiparticle energies were calculated using the standard BCS formula, with $\Delta = 1.66$ MeV, as derived from the odd-even mass differences defined in Ref. [27]. Although the $g_{9/2}$ shell is predicted to lie higher above the Fermi level in the Woods-Saxon and Hartree-Fock calculations then in the Nilsson model, this difference was apparently not great enough in magnitude to cause any significant disagreement between the Woods-Saxon and Nilsson models' calculations of the gamma softness of the minimum. Since the Hartree-Fock calculations explicitly include proton-neutron interactions, it is reassuring to note that the resulting levels are not drastically different from the other two sets. The three sets of calculations give single-particle spectra which are otherwise similar, including $N = 28$ and $Z = 28$ shell-gaps of 4–6 MeV.

It is also possible that the failure of the calculations is related to technical shortcomings of the Strutinsky approach. The limitations of the Strutinsky method, and some of the technical difficulties which may arise in Strutinsky calculations, are discussed in Ref. [28]. There are two main technical issues which may be relevant to the present difficulties. First, the liquid-drop energy and the Strutinsky shell correction correspond to the terms of order $\tilde{\rho}^2$ and $\tilde{\rho}\cdot\delta\rho$, respectively, in an expansion of the Hartree-Fock energy in the smooth and oscillating parts of the density matrix, $\rho = \tilde{\rho} + \delta\rho$. The term of order $\delta\rho^2$ has been shown numerically to be small in heavy nuclei, but is not negligible for A less than about 40–50 [28]. The second difficulty arises becuase in Strutinsky calculations, a prescription must be decided upon for dealing with continuum states. There is clearly a lack of self-consistency here. In the case of ^{64}Zn, the shape-driving proton $g_{9/2}$ shell is unbound at zero deformation, but bound for deformed shapes.

V. CONCLUSIONS

Cranked Strutinsky calculations have proven to be an extremely powerful tool in the interpretation of the high-spin structure of open-shell nuclei, for which tradiational shell-model calculations are not feasible. In cases where Strutinsky calculations predict a well-defined deformed minimum in the potential energy surface, they have seldom been proven wrong by experiment. The nucleus ^{64}Zn at high spin appears to be an egregious exception to this record of reliability. The present experiment has probed the structure of ^{64}Zn for the first time at spins above the first alignment of $g_{9/2}$ neutrons near $8\hbar$. The calculations predict that at these spins, the potential energy surface should become much more stable with respect to the nonaxially symmetric degrees of freedom, which should result in the appearance of well-defined rotational bands. The data appear to contradict this. The rotational band structure is less pronounced at high spins than at low spins. Possible reasons for this discrepancy have been suggested, the most likely being that difficulties are encountered in the Strutinsky method in nuclei whose Fermi level lies in a major shell which is truncated by the continuum, leading to a lack of consistency in the treatment of the shape-polarizing nonnatural-parity states. This is of clear relevance to the present experimental efforts to study the structures of nuclei far from stability.

TABLE IV. Location of the $g_{9/2}$ orbital as calculated in various spherical potentials.

	Single-particle energy relative to Fermi level (MeV)	Quasiparticle energy (MeV)
Nilsson	2.8	3.2
Woods-Saxon	4.1	4.4
Skyrme-Hartree-Fock	4.8	5.0

ACKNOWLEDGMENTS

The authors thank T. Bengtsson for making available to the nuclear physics community his code for performing cranked Nilsson-Strutinsky calculations, and W. Nazarewicz for the database of total Routhian surfaces for the $A \sim 80$ region. This work was supported in part by the Department of Energy, Nuclear Physics Division, under Grant No. DE-FG-02-91ER-40609 and Contract No. W-31-109-ENG-38.

[1] P. J. Nolan and P. J. Twin, Annu. Rev. Nucl. Part. Sci. **38**, 533 (1988).
[2] R. V. F. Janssens and T. L. Khoo, Annu. Rev. Nucl. Part. Sci. **41**, 321 (1991).
[3] B. Crowell, P. Chowdhury, D. J. Blumenthal, P. J. Ennis, S. J. Freeman, C. J. Lister, S. Smolen, and Ch. Winter, Phys. Rev. C **45**, 1564 (1992).
[4] V. P. Janzen *et al.*, Phys. Rev. Lett. **70**, 1065 (1993).
[5] P. Raghavan, At. Data Nucl. Data Tables **42**, 189 (1989).
[6] P. J. Ennis, C. J. Lister, W. Gelletly, H. G. Price, B. J. Varley, P. A. Butler, T. Hoare, S. Cwiok, and W. Nazarewicz, Nucl. Phys. A **535**, 392 (1991).
[7] R. H. Spear, At. Data Nucl. Data Tables **42**, 55 (1989).
[8] D. N. Simister, G. D. Jones, A. Kogan, P. R. G. Lornie, T. P. Morrison, O. M. Mustaffa, H. G. Price, P. J. Twin, and R. Wadsworth, J. Phys. G **4**, 111 (1978).
[9] D. N. Simister, G. D. Jones, F. Kearns, A. Kogan, P. R. G. Lornie, T. P. Morrison, O. M. Mustaffa, H. G. Price, P. J. Twin, and R. Wadsworth, J. Phys. G **4**, 1127 (1978).
[10] D. N. Simister, L. P. Ekström, G. D. Jones, F. Kearns, T. P. Morrison, O. M. Mustaffa, H. G. Price, P. J. Twin, R. Wadsworth, and N. J. Ward, J. Phys. G **6**, 81 (1980).
[11] L. Chaturvedi *et al.*, Phys. Rev. C **43**, 2541 (1991).
[12] K. S. Krane, R. M. Steffen, and R. M. Wheeler, Nucl. Data Tables **11**, 351 (1973).
[13] Chr. Bargholtz and P.-E. Tegnér, Nucl. Instrum. Methods A **256**, 513 (1987).
[14] T. Bengtsson, Nucl. Phys. A **496**, 56 (1989), and references therein.
[15] T. Bengtsson and I. Ragnarsson, Nucl. Phys. A **436**, 14 (1985).
[16] J. F. A. van Hienen, W. Chung, and B. H. Wildenthal, Nucl. Phys. A **269**, 159 (1976).
[17] S. Cwiok, J. Dudek, W. Nazarewicz, J. Skalsi, and T. Werner, Comput. Phys. Commun. **46**, (1987) 379.
[18] "Database of Total Routhian Surfaces," W. Nazarewicz (private communication).
[19] D. Troltenier, J. A. Maruhn, and P. O. Hess, in *Computational Nuclear Physics 1: Nuclear Structure*, edited by K. Langanke, J. A. Maruhn, and S. E. Koonin (Springer-Verlag, Berlin, 1991).
[20] N. V. Zamfir and R. F. Casten, Phys. Lett. B **260**, 265 (1991).
[21] A. S. Davydov and G. F. Filippov, Nucl. Phys. **8**, 237 (1958).
[22] C. W. Johnson, S. E. Koonin, G. H. Lang, and W. E. Ormand, Phys. Rev. Lett. **69**, 3157 (1992).
[23] J. Rekstad and G. Løvhøiden, Nucl. Phys. A **267**, 40 (1976).
[24] D. Galeriu, D. Bucurescu, and M. Ivascu, J. Phys. G **12**, 329 (1986); *Proceedings of the International Nuclear Physics Conference*, Harrogate, 1986, edited by G. C. Morrison (Institute of Physics, University of Reading, Berkshire, 1986).
[25] R. Bengtsson, J. Dudek, W. Nazarewicz, and P. Olanders, Phys. Scr. **39**, 196 (1989).
[26] P.-G. Reinhard, in *Computational Nuclear Physics 1: Nuclear Structure* [19].
[27] A. S. Jensen *et al.*, Nucl. Phys. A **431**, 393 (1984).
[28] M. Brack, in *Proceedings of International Workshop on Nuclear Structure Models*, Oak Ridge, March 1992, edited by R. Bengtsson, J. Draayer and W. Nazarewicz (World Scientific, Singapore, 1992).